

# Thick electrodes for electrochemical relithiation to regenerate spent battery powder

Yifan Gao<sup>a</sup>, Weiyin Chen<sup>a</sup>, Jin-Sung Park<sup>a</sup>, Hui Xu<sup>b</sup>, Tao Dai<sup>a</sup>, Xia Huang<sup>c</sup>, Ju Li<sup>a,d,\*</sup> 

<sup>a</sup> Department of Nuclear Science and Engineering, Massachusetts Institute of Technology, 77 Massachusetts Avenue, Cambridge, MA 02139, USA

<sup>b</sup> Department of Materials Science and Engineering, Shanghai Institute of Technology, 100 Haiquan Road, Fengxian District, Shanghai, 201418, PR China

<sup>c</sup> State Key Joint Laboratory of Environment Simulation and Pollution Control, School of Environment, Tsinghua University, Beijing 100084, PR China

<sup>d</sup> Department of Materials Science and Engineering, Massachusetts Institute of Technology, 77 Massachusetts Avenue, Cambridge, MA 02139, USA

## ARTICLE INFO

### Keywords:

Direct regeneration  
Spent batteries  
LiFePO<sub>4</sub> cathode  
Battery recycling  
Electrochemical relithiation

## ABSTRACT

The growing use of lithium iron phosphate (LiFePO<sub>4</sub>, LFP) batteries in electric vehicles and energy storage systems highlights the urgent need for efficient and sustainable recycling methods. Direct recovery technologies show promise but often require supplementary lithium chemicals. This study introduces a thick electrode system for the electrochemical relithiation of spent LFP battery powder, utilizing residual lithium from low-grade Black Mass. Unlike previous regeneration techniques, this method eliminates the need for external lithium sources beyond the spent battery powder and the minimal amount of aqueous electrolyte. Our approach overcomes the limitations of traditional electrochemical relithiation by directly processing the spent battery powder without binder, enhancing both industrial scalability and processing capacity. The thick electrode system significantly improves powder recovery capacity, achieving 405 g h<sup>-1</sup> m<sup>-2</sup> with low energy consumption (9.3 kWh t<sup>-1</sup>), and demonstrates excellent performance subsequently. Ecological and economic assessments reveal considerable reductions in the recycling cost and environmental impact.

## 1. Introduction

The rapid adoption of lithium-ion batteries [1–4] across a wide range of applications, from electric vehicles to energy storage systems [5,6], has created an urgent need for efficient and sustainable recycling methods [7–10]. Lithium iron phosphate (LiFePO<sub>4</sub>, LFP) batteries are projected to hold the largest share of the global battery market in the coming years [11,12] and have already overtaken nickel cobalt manganese (NCM) batteries in Asia [13]. Once lithium-ion batteries reach the end of their life cycle (capacity < 80 %) [10], they pose significant environmental risks if not properly recycled, along with the loss of valuable resources [14]. Recycling not only reduces environmental harm but also recovers critical resources, contributing to sustainability in battery use [6,10,15–17].

Current industrial recycling methods, primarily pyrometallurgical and hydrometallurgical processes [14,18,19], face several challenges, including high energy consumption, significant CO<sub>2</sub> emissions, waste generation, and lengthy procedures to recover LFP cathodes [6]. While these methods can recover metals such as lithium [20], cobalt, and nickel [21], the recovered materials often require extensive

processing—extraction, precipitation, separation, and annealing [18]—before they can be reused in battery manufacturing. Recent research has increasingly shifted towards direct regeneration methods [8,9,22–25], which aim to preserve the structural integrity of cathode materials and reduce the need for synthesizing new materials from recovered metals [26]. In fact, the degradation of most battery cathodes is primarily due to lithium depletion [27]. Therefore, the key to direct regeneration lies in replenishing lithium (relithiation) while maintaining the crystal structure of the cathode [27–29]. However, these methods typically require external lithium sources to replenish lithium content, which increases both the cost and carbon footprint. Additionally, direct regeneration processes are not compatible with the most common industrial “Black Mass”, the mixed powder from spent cathodes and anodes, limiting their ability to fully utilize valuable resources. The electrochemical lithium recovery method [30–33] is based on the selective dissolution and intercalation of lithium ions under current, which enables lithium extraction and replenishment. However, current proposed electrochemical methods [34,35] require additional steps of binding the powder as an electrode and turning the electrode into powder again after electrochemical process, making it impossible to

\* Corresponding author.

E-mail address: [liju@mit.edu](mailto:liju@mit.edu) (J. Li).

<https://doi.org/10.1016/j.ensm.2025.104269>

Received 29 January 2025; Received in revised form 11 April 2025; Accepted 18 April 2025

Available online 19 April 2025

2405-8297/© 2025 Elsevier B.V. All rights are reserved, including those for text and data mining, AI training, and similar technologies.

directly process waste battery powder.

In this study, we developed a novel thick electrode system for the electrochemical relithiation of spent LFP battery powder. This approach utilizes the residual lithium present in low-grade Black Mass, to replenish the lithium deficit in spent LFP powders, achieving this with minimal electrical energy, a minimal amount of lithium aqueous electrolyte, and without the need for external lithium sources. The electrochemically relithiated powder is then heat-treated to repair the LFP olivine structure without the additional lithium source. Unlike previous electrochemical relithiation methods [32–36], which require binder-based electrode fabrication, our binder-free method uses sandwich thick electrodes, enabling direct processing of the spent powder and direct production of regenerated powder. This simplifies loading and unloading, making the system more suitable for industrial assembly line operations (Fig. 1a). With electrode thicknesses 10 to 30 times greater than conventional battery electrodes, the system significantly increases the powder recovery capacity to  $405 \text{ g h}^{-1} \text{ m}^{-2}$  under low energy consumption ( $9.3 \text{ kWh t}^{-1}$ ). Additionally, we found that constant current relithiation outperforms constant voltage relithiation. Ecological and economic evaluations suggest that this thick electrode method could lower the costs of battery regeneration while reducing environmental impacts.

## 2. Results and discussion

### 2.1. Feasibility of regenerating spent batteries using thick electrodes

Unlike conventional battery regeneration techniques, we propose an assembly line process for battery regeneration based on thick electrodes (Fig. 1a and 1b). As shown in Fig. 1a, the process involves sequentially

loading spent LFP (S-LFP) cathode powder and Black Mass powder into two stacked thick electrodes separated by a lithium ion ( $\text{Li}^+$ )-permeable separator (Fig. 1b). The electrode loaded with Black Mass acts as the anode (mass loading  $\sim 41 \text{ mg cm}^{-2}$ ), while the S-LFP-loaded electrode functions as the cathode (mass loading  $\sim 101 \text{ mg cm}^{-2}$ ) in the thick electrodes setup (Fig. 1b and Fig. S1) for electrochemical relithiation. When a constant current is applied,  $\text{Li}^+$  migrates from the Black Mass at the anode and intercalate into the S-LFP at the cathode, thereby replenishing its lithium content (Fig. 1b). This migration and intercalation process is monitored by tracking the cell voltage over time, as shown in Fig. 1c. The voltage required for relithiation increases gradually until it reaches a pre-set cut-off value.

After reaching the cut-off voltage, the powder from the thick electrodes is unloaded by relieving pressure and simply scraping after drying. The powder from the cathode side undergoes a two-hour annealing process at  $600^\circ\text{C}$  (Fig. 1a) in an inert argon atmosphere to repair and stabilize the olivine structure of LFP. This calcination step could also remove the cathode electrolyte interphase, binder, and other impurities from the spent battery powder. To evaluate lithium replenishment across the entire electrode, the final product, regenerated LFP (R-LFP) was fully collected, homogenized, and subjected to Inductively Coupled Plasma Optical Emission Spectroscopy (ICP-OES) analysis (Fig. 1d and Supplementary Note 1). The R-LFP restores the Li/Fe and Li/P ratios to 1, identical to those of freshly synthesized LFP (F-LFP). These values represent the average composition of the entire electrode volume, indicating that complete relithiation was achieved throughout the thick electrode. Besides, the Fe/P ratio remained close to 1 across all samples, confirming that the Fe–P framework of LFP was well preserved during the regeneration process. The first charge capacity of the coin cell batteries assembled from the R-LFP, S-LFP, and F-LFP powders directly

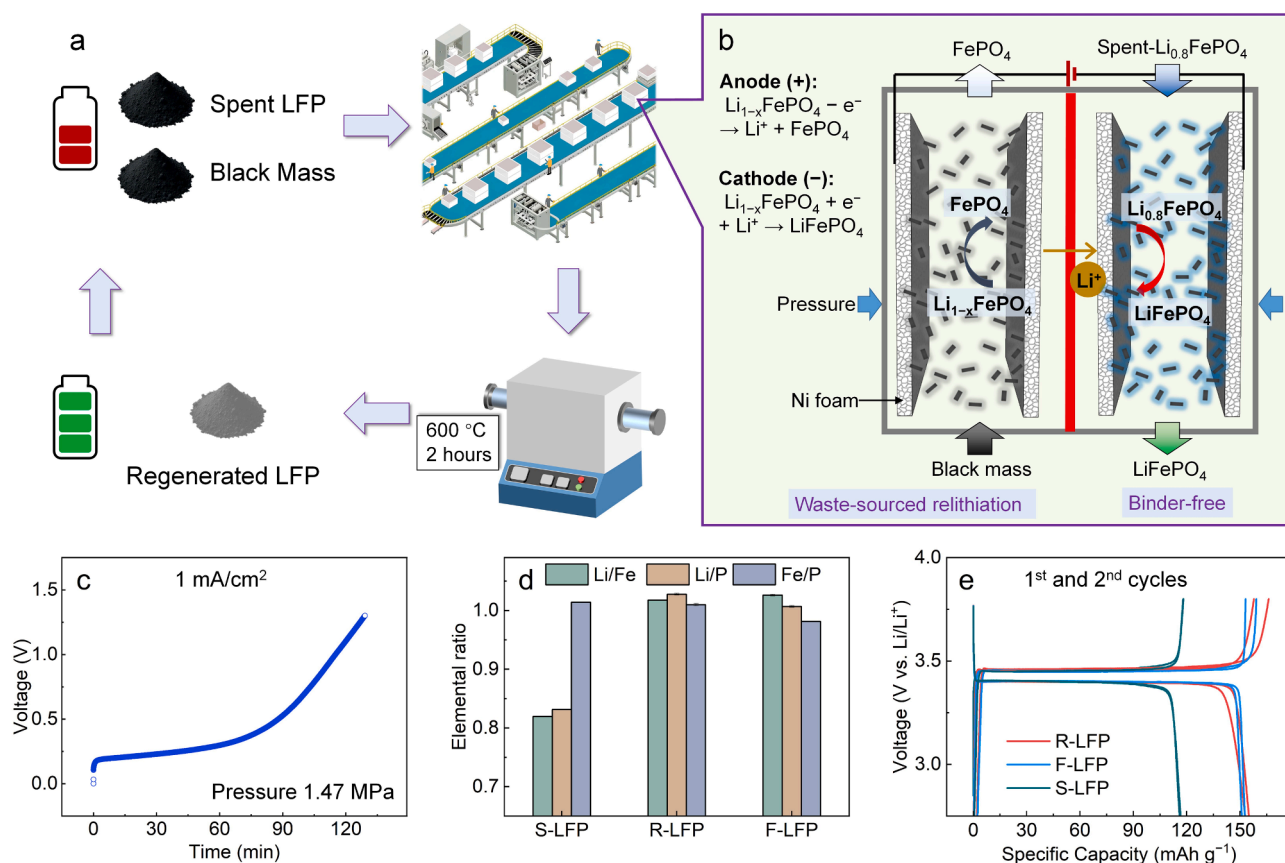


**Fig. 1.** Regeneration process using thick electrodes. (a) Schematic illustration of the regeneration process for spent batteries using thick electrodes; (b) Schematic of the electrochemical relithiation process utilizing thick electrodes; (c) Cell voltage versus time during the constant-current electrochemical relithiation process; (d) Li/Fe, Li/P, and Fe/P ratios of different  $\text{LiFePO}_4$  (LFP) powders; (e) First and second cycle performance of different LFP powders tested with coin cells.

reflects the lithium content. As shown in Fig. 1e, the first charge capacity of S-LFP is only  $118.2 \text{ mAh g}^{-1}$ , significantly lower than the  $159.2 \text{ mAh g}^{-1}$  of F-LFP. On the other hand, the first charge capacity of R-LFP is  $166.1 \text{ mAh g}^{-1}$ , which is even a bit higher than that of F-LFP. The high capacity comparable to F-LFP, as well as charge/discharge cycles, demonstrated the completion of electrochemical relithiation and the olivine structural repair by subsequent heat treatment. A detailed analysis of impurity content in the R-LFP, S-LFP, and black mass is provided in Table S1 and Supplementary Note 2. The impurity levels in R-LFP remain as low as those in S-LFP, with only trace amounts of aluminum ( $\sim 0.21 \text{ wt } \%$ ) detected in both samples, indicating minimal contamination during the regeneration process. These results demonstrate that lithium-deficient S-LFP was successfully regenerated into R-LFP, confirming the feasibility of using thick electrode technology for spent battery regeneration.

## 2.2. Electrochemical performance and characterization of LiFePO<sub>4</sub>

The electrochemical stability of R-LFP exhibit good performance, as shown in Fig. 2a, which compares the specific capacity over multiple consecutive charge/discharge cycles for R-LFP, F-LFP, and S-LFP. R-LFP exhibits stability comparable to F-LFP, with significantly better performance than S-LFP. The R-LFP retained 97 % of its initial capacity over 100 cycles, corresponding to a capacity fade of  $\sim 0.03 \%$  per cycle. Based on this trend, the projected capacity would remain at approximately  $128.8 \text{ mAh g}^{-1}$  after 500 cycles. Throughout the cycling process, R-LFP maintains a Coulombic efficiency close to 99.9 %, indicating minimal lithium ion loss during charge-discharge cycles. In the rate performance tests shown in Fig. 2b, R-LFP outperforms S-LFP, further demonstrating its superior electrochemical properties. To further evaluate the electrochemical behavior, cyclic voltammetry (CV), electrochemical impedance spectroscopy (EIS), and galvanostatic intermittent titration technique (GITT) measurements were performed (Fig. S2). The CV profiles of R-LFP exhibit well-defined redox peaks closely matching those of F-LFP, indicating successful restoration of redox activity. EIS analysis shows comparable charge transfer resistance between R-LFP and F-LFP. GITT results further confirm that the lithium-ion diffusion behavior of R-LFP is similar to that of F-LFP, supporting the preservation

of transport kinetics after regeneration. The similarity in cycling behavior, rate capability, CV, EIS, and GITT responses between R-LFP and F-LFP further validates the effectiveness of the relithiation process.

Further evaluation of the electrochemical relithiation process highlights significant advantages in both energy consumption ( $\text{kWh t}^{-1}$ ) and recycling capacity ( $\text{g h}^{-1} \text{ m}^{-2}$ ). As shown in Fig. 2c, this study achieves the highest production capacity ( $405 \text{ g h}^{-1} \text{ m}^{-2}$ ) with the lowest energy consumption ( $9.3 \text{ kWh t}^{-1}$ ) compared to previously reported works (See Table S2 for details [32,33,36–41]). Additional parameters, including CO<sub>2</sub> equivalent emissions from electricity cost ( $\text{kg t}^{-1}$ ), discharge capacity of the regenerated LFP ( $\text{mAh g}^{-1}$ ), binder requirement, and lithium source, were also considered to enable a more comprehensive comparison (Table S2). Most previously reported electrochemical relithiation methods rely on binder-containing electrodes, but their electrochemical performance is lower than that of our binder-free thick electrodes system. These additional dimensions further highlight the electrochemical and environmental advantages of our system. These improvements are attributed to the use of binder-free, highly porous thick electrodes, which enable the electrochemical relithiation of large amounts of battery powder by facilitating both lithium-ion transport and uniform current distribution across the entire electrode. The spent LFP powder already contains conductive carbon, which ensures sufficient electronic conductivity throughout the electrode without the need for additional conductive additives. The large porosity of the binder-free thick electrodes ensures fast ion transport, enabling electrochemical accessibility even in deep electrode regions and allowing complete relithiation despite the high thickness. In contrast, earlier electrochemical relithiation methods relied on conventional systems with thin or slurry electrodes submerged in large solution volumes, resulting in limited powder processing capacity and higher energy consumption.

X-ray diffraction (XRD) analysis, shown in Fig. 2d, confirms the successful regeneration of R-LFP, with a pattern identical to that of F-LFP. In contrast, S-LFP displays additional peaks corresponding to FePO<sub>4</sub>, indicating lithium deficiency. X-ray photoelectron spectroscopy (XPS) results in Fig. 2e further validate the regeneration, showing that R-LFP and F-LFP predominantly contain divalent iron ( $\text{Fe}^{2+}$ ), whereas S-LFP contains trivalent iron ( $\text{Fe}^{3+}$ ). The in-depth Fe 2p XPS spectrum of R-LFP (Fig. 2f) reveals that the interior of R-LFP is primarily composed

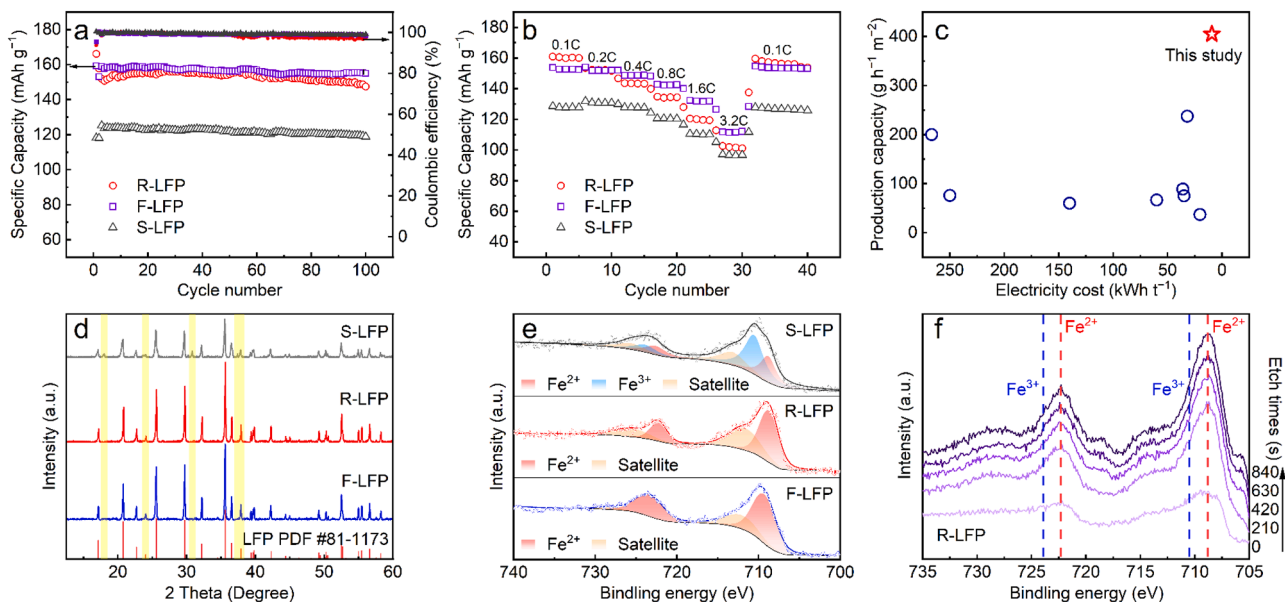


**Fig. 2.** Electrochemical performance and characterization of R-LFP, F-LFP, and S-LFP. (a) Charge and discharge cycles for R-LFP, F-LFP, and S-LFP; (b) Rate performance test results for R-LFP, F-LFP, and S-LFP; (c) Comparison of electrical energy consumption ( $\text{kWh t}^{-1}$ ) and production capacity ( $\text{g h}^{-1} \text{ m}^{-2}$ ) of R-LFP in this work versus other electrochemical relithiation studies (See Table S2 for details); (d) XRD patterns of S-LFP, R-LFP, and F-LFP; (e) Fe 2p XPS spectra for S-LFP, R-LFP, and F-LFP; (f) In-depth Fe 2p XPS spectrum of R-LFP.

of  $\text{Fe}^{2+}$ . While some surface  $\text{Fe}^{2+}$  may be slightly affected by air oxidation, the internal  $\text{Fe}^{2+}$  confirms the full regeneration of the  $\text{LiFePO}_4$  structure. This analysis, corroborated by scanning electron microscopy (SEM) and transmission electron microscopy (TEM) images (Fig. S3a–3d), shows the regenerated microstructure of R-LFP.

### 2.3. Difference between the constant-current and constant-voltage relithiation

Electrochemical relithiation can be conducted using either constant-voltage or constant-current methods. In this study, we compared the electrochemical relithiation of S-LFP based on thick electrodes using both approaches. Fig. 3a and 3b display the voltage and current profiles, for relithiation under constant-current and constant-voltage conditions. In the constant-voltage method, the current decreases rapidly, indicating a swift decline in relithiation efficiency over time, whereas the voltage rise under constant-current conditions is more gradual. Based on the ICP results (Fig. 3c), constant-current relithiation successfully restores the Li/Fe and Li/P ratios in S-LFP to above 1, indicating complete lithium replenishment. In contrast, constant-voltage relithiation only achieves Li/Fe and Li/P ratios of  $\sim 0.75$ , suggesting its relative inefficiency. Additionally, the lithium content in the anodic Black Mass decreases significantly more in the constant-current method compared to the constant-voltage approach, further demonstrating that constant-current relithiation is more effective at migrating  $\text{Li}^+$  from the anode to the cathode. It is worth noting that the initial Li/Fe ratio of Black Mass is close to 1. This is because Black Mass is a mixture of waste cathode and anode powder, so the “dead lithium” on the anode is also included.

The superiority of constant-current relithiation is primarily due to its control over the reaction kinetics. In constant-current mode (Fig. 3a), the current directly governs the kinetics of the relithiation process, allowing for more consistent performance. This mode brings the system closer to thermodynamic equilibrium, making it less susceptible to kinetic limitations. Therefore, the relithiation results can be affected by the kinetics of the reaction, which can be controlled under the constant-current mode. While in the constant-voltage mode (Fig. 3b), the initial excessive current may lead to the damage of the LFP olivine structure [42], which prevents the subsequent electrochemical intercalation of

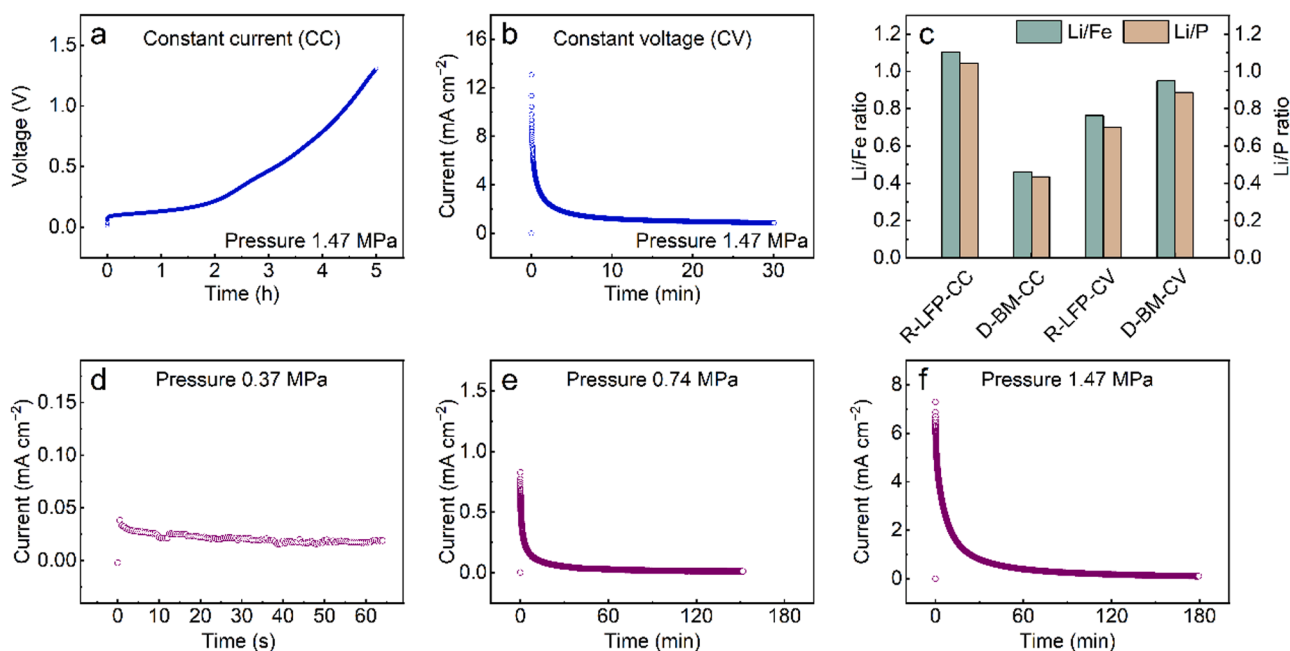
lithium. This could be the reason for the rapid drop in current in the constant-voltage mode.

But the constant-voltage mode is suitable for system optimization. The effectiveness of Li-ion migration can be directly assessed by observing the magnitude and variation of the current under a constant voltage. We optimized the pressure applied to both sides of the thick electrodes using the constant-voltage mode (Fig. 3d–3f). The current increases with applied pressure from 0.37 MPa to 1.47 MPa, indicating that higher pressure enhances lithiation kinetics by reducing electrical resistance between powder particles and facilitating more effective lithium intercalation into S-LFP. However, applying pressure beyond 1.47 MPa risks short-circuiting due to particle penetration through the separator. In addition, excessive pressure sharply reduces the porosity of the electrode, which can lead to electrolyte being expelled from the electrode structure and result in impaired ionic transport pathways. Therefore, 1.47 MPa is considered the optimal applied pressure in this system.

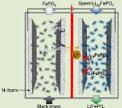
In addition to pressure, we optimized other parameters, including the current collector material (nickel foam or carbon felt, Fig. S4), electrolyte volume (Fig. S5), electrolyte Li-ion concentration (Fig. S6), the amount of powder loading (Fig. S7), and the type of separator (Fig. S8). The optimized thick electrode system achieves rapid and large-scale regeneration of S-LFP with minimal energy consumption. The amount of powder loaded on the thick electrode system can be calculated and balanced in the future based on the Li/Fe ratio of S-LFP and Black Mass to further improve the lithium utilization of the Black Mass.

### 2.4. Ecological and economic evaluation

A comparative ecological and economic evaluation of our approach against conventional recycling methods—including aqueous direct regeneration, annealing direct regeneration, and industrial hydrometallurgical recycling—demonstrates significant advantages (Fig. 4). We based our assessment on a previous study’s ecological and economic evaluation [43] of common repair methods for producing 1 ton of functional LFP from industrial spent LFP powder. For each recycling technology, factors such as feedstock price ( $\sim \$730$ /ton S-LFP) and  $\text{CO}_2$



**Fig. 3.** Comparison of relithiation performance using constant-current (CC) versus constant-voltage (CV). (a) Cell voltage versus time during the CC ( $I = 1 \text{ mA cm}^{-2}$ ) relithiation process. (b) Current versus time during the CV ( $V = 0.3 \text{ V}$ ) relithiation process. (c) Li/Fe and Li/P ratios of different powders, BM: Black Mass, D-BM: delithiated BM. (d–f) Effect of applied pressure on the electrochemical relithiation process under CV mode ( $V = 0.3 \text{ V}$ ).

For per ton LFP	Pre-processing	Relithiation	Post-processing	Total /t LFP
<b>This work</b> 	+ 0.4 t Black mass (\$292) + Electrolyte (\$35) + Separator (\$27) Powder loading electricity (20 kWh, \$2)	Electricity 9.3 kWh (\$0.9) Annealing (600°C 2h, ~27 MJ/kg) +922 m <sup>3</sup> LNG (\$460) +55 m <sup>3</sup> N <sub>2</sub> (\$4.4) Direct CO <sub>2</sub> e (0.083) Energy CO <sub>2</sub> e (1.644)	Tail gas treatment (\$25) Separation & Maintenance etc. (\$300+20kWh (\$2)) CO <sub>2</sub> e (0.016)	CO <sub>2</sub> e: 1.9  Cost: \$1878
<b>Aqueous direct regeneration</b> 	+ 7kg Li <sub>2</sub> CO <sub>3</sub> (\$68) + 55kg LiOH (\$597) + 20kg citric acid (\$100)	Heating (60-80 °C 6-12h) or Electrochemical Reaction (8h) +Electricity (~166 kWh) (\$17 / CO <sub>2</sub> e 0.132) +Utilities etc. (\$115)	Annealing (500°C 2h, ~25 MJ/kg) +1025 m <sup>3</sup> LNG (\$513) +60 m <sup>3</sup> N <sub>2</sub> (\$4.8) Energy CO <sub>2</sub> e (1.826) Maintenance (\$530)	CO <sub>2</sub> e: 2.1  Cost: \$2675
<b>Annealing direct regeneration</b> 	+ 49kg Li <sub>2</sub> CO <sub>3</sub> (\$476) + 62.5 kg sugar (\$15)  Mixing (\$10) CO <sub>2</sub> e (0.008)	Annealing (600°C 4h, ~54 MJ/kg)  +1844 m <sup>3</sup> LNG (\$922) +110 m <sup>3</sup> N <sub>2</sub> (\$8.8) Direct CO <sub>2</sub> e (0.166) Energy CO <sub>2</sub> e (3.288)	Tail gas treatment (\$25) Separation & Maintenance etc. (\$300+20kWh (\$2)) CO <sub>2</sub> e (0.016)	CO <sub>2</sub> e: 3.6  Cost: \$2489
<b>Hydrometallurgical recycle and re-synthesis</b> 	+ 20% extra spent LFP cost (\$146 / CO <sub>2</sub> e 0.024) 0.75t H <sub>2</sub> SO <sub>4</sub> ~4h Leaching (\$150) Filtration & Calcination (\$270) CO <sub>2</sub> e (0.994) direct CO <sub>2</sub> e (0.048)	Annealing (750°C 8h, ~105 MJ/kg)  +3586 m <sup>3</sup> LNG (\$1793) +195 m <sup>3</sup> N <sub>2</sub> (\$15.6) Energy CO <sub>2</sub> e (6.393) direct CO <sub>2</sub> e (0.143) +0.95 t new FePO <sub>4</sub> (\$1391)	By-product revenue (-\$240)  Maintenance etc. (\$450+30 kWh (\$3)) CO <sub>2</sub> e (0.024)	CO <sub>2</sub> e: 7.7  Cost: \$4709

**Fig. 4.** Cost assessment of our thick electrode against conventional recycling methodologies. This includes pre-processing steps such as raw material prices, powder loading, mixing, and leaching; the relithiation process including electricity, annealing, heating, and fuel; and post-treatment procedures like tail gas treatment, separation, maintenance, and by-product revenue. The average market prices surveyed in September 2024 was used. CO<sub>2</sub>e: CO<sub>2</sub> equivalent.

equivalent (CO<sub>2</sub>e, 0.121) of the S-LFP, the pre-processing, relithiation process, and the post-treatment process, etc., were all included in the cost assessment. The results show that the thick electrode method in this study excels in both reducing economic costs and minimizing CO<sub>2</sub> emissions, representing a significant advancement in sustainable battery material recycling.

A detailed analysis (see **Supplementary Note 3**), covering every stage from spent LFP battery processing to the production of functional cathode materials, highlights the superior ecological footprint of our method. By optimizing energy consumption and reducing hazardous emissions—from 7.7 CO<sub>2</sub> equivalent to 1.9 CO<sub>2</sub> equivalent—this approach addresses the urgent need for greener recycling technologies and aligns with global sustainability goals. Moreover, the economic viability is evident from the significant reduction in processing costs (\$1878) compared to traditional methods (\$4709), ensuring maximum material reuse with minimal energy input. Furthermore, the thick electrode system presented in this work can be applied not only to battery regeneration but also to other electrochemical processes involving electrolyte-solid phase active materials, such as aqueous batteries and electroplating industries.

### 3. Conclusion

In summary, this study developed a binder-free thick electrode system for the electrochemical relithiation of spent LFP battery powders, utilizing residual lithium from low-grade Black Mass. This method effectively replenishes lithium in spent LFP without requiring external lithium sources, apart from the minimal in the aqueous electrolyte, thereby enhancing recovery efficiency and simplifying processing. The system is well-suited for scaled-up industrial application. The thick electrode design allows for increased powder recovery per unit area (405 g h<sup>-1</sup> m<sup>-2</sup>) with minimal energy consumption (9.3 kWh t<sup>-1</sup>). The demonstrated superiority of constant-current relithiation over constant-voltage relithiation further advances the development of electrochemical relithiation methods. Ecological and economic evaluations confirm the potential of this approach to significantly reduce recycling costs and environmental impact, contributing to a more sustainable battery lifecycle. This work introduces a promising new approach to

battery recycling, supporting global sustainability goals and advancing the circular economy.

## 4. Experimental section

### 4.1. Chemicals and spent LIBs

The black mass powder and S-LFP powder were sourced from Jiecheng New Energy Company. The F-LFP was purchased from MTI Corporation (Richmond, CA, USA) under product ID LIB-LFPO. It is a carbon-coated LFP powder designed for use as a cathode material in lithium-ion batteries. The D50 particle size is 3.5 ± 1.0 μm. The elemental composition includes 4.40 ± 0.50 wt % Li, 34.5 ± 1.0 wt % Fe, and 19.5 ± 1.0 wt % P. The main components of S-LFP, F-LFP, and Black Mass are listed in **Table S3**, showing Li:Fe molar ratios of 0.82:1, 1.03:1, and 0.99:1, respectively. The received spent battery powder was used in the research without any additional pretreatment. All chemical reagents were of analytical grade and purchased from Sigma-Aldrich.

### 4.2. Powder loading of thick electrodes

In assembling thick electrodes, the process began by placing a nickel foam current collector into a custom cell case with grooves. A specific amount of S-LFP powder was uniformly distributed over the surface of the collector. Next, a specified volume of aqueous electrolyte solution, containing lithium nitrate (LiNO<sub>3</sub>) at a Li<sup>+</sup> concentration of 2 g L<sup>-1</sup>, was added to fully immerse the powder. Another piece of nickel foam was placed on top, completing the cathodic thick electrode assembly. A separator was then positioned over the current collector. A similar procedure was followed for assembling the anode thick electrode. A second grooved cell case was placed above, with nickel foam serving as the current collector. Black Mass powder was evenly distributed over the current collector, followed by a specified volume of the aqueous LiNO<sub>3</sub> electrolyte solution. To enclose the thick electrodes of both the cathode and anode, two steel plates were positioned on the outer sides, and a predefined mechanical pressure was applied. The final assembly is shown in **Fig. 1b**.

### 4.3. Regeneration process of electrochemical relithiation

During electrochemical relithiation, either a constant current or constant voltage was applied using an electrochemical workstation (Gamry Reference 600+). After relithiation, the powders from both the cathodic electrode (loaded with S-LFP for relithiation) and the anodic electrode (loaded with Black Mass for delithiation) were easily scraped off with a spoon and placed in an oven at 100 °C for drying. Following drying, the powder from the cathode (post-lithiation) was calcined under an argon atmosphere at 600 °C for 2 h. The calcined powder is considered regenerated and is referred to as R-LFP.

### 4.4. Materials characterizations

The elemental contents of Li, Fe and P were analyzed using inductively coupled plasma optical emission spectroscopy (ICP-OES, Agilent 7900). The phase compositions of the samples were characterized by X-ray diffraction (XRD, PANalytical, AERIS, Cu K $\alpha$  radiation). The elemental valence states were examined using X-ray photoelectron spectroscopy (XPS, PHI Versaprobe II, Physical Electronics). The morphology of the samples was evaluated by scanning electron microscopy (SEM, Phenom Pharos G2, Zeiss Merlin) and transmission electron microscopy (TEM, FEI Tecnai G2 Spirit TWIN, Thermo Fisher). The applied pressure was measured with a Fujifilm pressure indicating film. Cyclic voltammetry (CV) and electrochemical impedance spectroscopy (EIS) were performed using an electrochemical workstation. The galvanostatic intermittent titration technique (GITT) was performed by applying a series of constant current pulses (0.1C) for 20 min, each followed by a relaxation period of 3 h. The measurements were carried out in a two-electrode configuration, using a Li metal sheet as both the reference and counter electrode. The apparent lithium-ion diffusion coefficient ( $D_{Li^+}$ ) was calculated based on Fick's second law of diffusion in the single-phase region, using the following equation:

$$D_{Li^+} = \frac{4}{\pi\tau} \left( \frac{m_B V_m}{M_B A} \right)^2 \left( \frac{\Delta E_s}{\Delta E_t} \right)^2 \tau \ll \frac{L^2}{D_{Li^+}}$$

where:  $m_B$  is the mass of the active material in the electrode,  $V_m$  is the molar volume of the active material,  $M_B$  is the molecular weight of the active material,  $A$  is the active surface area between the electrode and the electrolyte,  $\Delta E_s$  is the steady-state voltage change during relaxation,  $\Delta E_t$  is the total transient voltage change during the current pulse,  $\tau$  is the duration of the current pulse,  $L$  is the effective diffusion length of  $Li^+$  ions. This approach allows for quantifying  $Li^+$  diffusion coefficients.

### 4.5. Electrochemical performance tests

The electrochemical properties of R-LFP, S-LFP, and F-LFP were evaluated using CR2032 coin cells. The electrode slurry was prepared by mixing LFP, carbon black and PVDF in NMP at a mass ratio of 8:1:1, then applied to aluminum foil. The electrodes were dried in a vacuum oven at 100 °C. Li/LFP coin cells were assembled using 1 M  $LiPF_6$  in an EC:DMC:DEC (1:1:1) electrolyte and a Celgard 2325 separator, inside an Ar-filled glove box ( $O_2$  content < 0.2 ppm,  $H_2O$  content < 0.01 ppm). The cells were tested using a LANHE battery working station system at 25 °C over a voltage range of 2.5–3.8 V. All electrochemical tests were performed after allowing the cells to rest for 6 h.

### 4.6. Economic and ecological assessment

The overall cost and  $CO_2$  equivalent (in kg per kg LFP, representing the equivalent  $CO_2$  emissions for producing 1 kg of functional LFP, excluding impurities) were evaluated using process-based models (see **Supplementary Note 3** for details). These models encompass every step, from spent LFP batteries to functional LFP cathode material based on related literature [43].

## CRediT authorship contribution statement

**Yifan Gao:** Writing – original draft, Methodology, Investigation, Formal analysis, Data curation, Conceptualization. **Weiyin Chen:** Writing – review & editing, Investigation. **Jin-Sung Park:** Writing – review & editing, Investigation. **Hui Xu:** Investigation. **Tao Dai:** Writing – review & editing, Investigation. **Xia Huang:** Writing – review & editing. **Ju Li:** Writing – review & editing, Supervision, Resources, Project administration, Investigation, Funding acquisition, Conceptualization.

## Declaration of competing interest

The authors declare that they have no known competing financial interests or personal relationships that could have appeared to influence the work reported in this paper.

## Acknowledgements

The authors would like to thank Dr. Yaoshen Niu from MIT for helping with the electrochemical characterization investigations and Dr. Jiadong Yu from Tsinghua University for discussions. The authors gratefully acknowledge the financial support from the National Natural Science Foundation of China (NSFC 52201267) and the Shanghai Sailing Program (22YF1447700).

## Supplementary materials

Supplementary material associated with this article can be found, in the online version, at [doi:10.1016/j.ensm.2025.104269](https://doi.org/10.1016/j.ensm.2025.104269).

## Data availability

Data will be made available on request.

## References

- [1] J. Niu, A. Kushima, X. Qian, L. Qi, K. Xiang, Y.M. Chiang, J. Li, Situ observation of random solid solution zone in  $LiFePO_4$  electrode, *Nano Lett.* 14 (2014) 4005–4010, <https://doi.org/10.1021/nl501415b>.
- [2] Lithium Iron Phosphate Set To Be The Next Big Thing In EV Batteries, (n.d.). <https://www.forbes.com/sites/samabuelsamid/2023/08/16/lithium-iron-phosphate-set-to-be-the-next-big-thing-in-ev-batteries/> (accessed June 20, 2024).
- [3] X.G. Yang, T. Liu, C.Y. Wang, Thermally modulated lithium iron phosphate batteries for mass-market electric vehicles, *Nat. Energy* 6 (2021) 176–185, <https://doi.org/10.1038/s41560-020-00757-7>.
- [4] Y. Huang, Y. Dong, Y. Yang, T. Liu, M. Yoon, S. Li, B. Wang, E.Y. Zheng, J. Lee, Y. Sun, Y. Han, J. Ciston, C. Ophus, C. Song, A. Penn, Y. Liao, H. Ji, T. Shi, M. Liao, Z. Cheng, J. Xiang, Y. Peng, L. Ma, X. Xiao, W.H. Kan, H. Chen, W. Yin, L. Guo, W. R. Liu, R. Muruganantham, C.C. Yang, Y. Zhu, Q. Li, J. Li, Integrated rocksalt–polyanion cathodes with excess lithium and stabilized cycling, *Nat. Energy* 2024) 1–9, <https://doi.org/10.1038/s41560-024-01615-6>.
- [5] Lithium Iron Phosphate Battery Market Size & Growth [2032], (n.d.). <https://www.fortunebusinessinsights.com/lithium-ion-li-ion-phosphate-batteries-market-102152> (accessed June 20, 2024).
- [6] Y. Huang, J. Li, Key challenges for grid-scale lithium-ion battery energy storage, *Adv. Energy Mater.* 12 (2022) 2202197, <https://doi.org/10.1002/aenm.202202197>.
- [7] W. Chen, J. Chen, K.V. Bets, R.V. Salvatierra, K.M. Wyss, G. Gao, C.H. Choi, B. Deng, X. Wang, J.T. Li, C. Kittrell, N. La, L. Eddy, P. Scotland, Y. Cheng, S. Xu, B. Li, M.B. Tomson, Y. Han, B.I. Yakobson, J.M. Tour, battery metal recycling by flash joule heating, *Sci. Adv.* 9 (2023) eadh5131, <https://doi.org/10.1126/sciadv.adh5131>.
- [8] G. Ji, J. Wang, Z. Liang, K. Jia, J. Ma, Z. Zhuang, G. Zhou, H.M. Cheng, Direct regeneration of degraded lithium-ion battery cathodes with a multifunctional organic lithium salt, *Nat. Commun.* 14 (2023) 584, <https://doi.org/10.1038/s41467-023-36197-6>.
- [9] V. Gupta, X. Yu, H. Gao, C. Brooks, W. Li, Z. Chen, Scalable direct recycling of cathode black mass from spent lithium-ion batteries, *Adv. Energy Mater.* 13 (2023) 2203093, <https://doi.org/10.1002/aenm.202203093>.
- [10] P. Xu, D.H.S. Tan, B. Jiao, H. Gao, X. Yu, Z. Chen, A materials perspective on direct recycling of lithium-ion batteries: principles, challenges and opportunities, *Adv. Funct. Mater.* 33 (2023) 2213168, <https://doi.org/10.1002/adfm.202213168>.
- [11] C. Price, Growing LFP adoption drives need for more transparency across chemistry's supply chain, *Fastmarkets* (2023). <https://www.fastmarkets.com/i>

- nsights/growing-lfp-adoption-drives-need-for-more-transparency-across-chemistrys-supply-chain/. accessed June 20, 2024.
- [12] A. Colthorpe, LFP to dominate 3TWh global lithium-ion battery market by 2030, *Energy-StorageNews* (2022). <https://www.energy-storage.news/lfp-to-dominate-3twh-global-lithium-ion-battery-market-by-2030/>. accessed June 20, 2024.
- [13] LFP batteries extend dominance over NCM batteries in China, *Fastmarkets* (2023). <https://www.fastmarkets.com/insights/lfp-batteries-extend-dominance-over-ncm-batteries-china/> (accessed June 20, 2024).
- [14] X. Zhang, M. Zhu, Recycling spent lithium-ion battery cathode: an overview, *Green Chem* (2024), <https://doi.org/10.1039/D4GC01781A>.
- [15] Y. Kong, L. Yuan, Y. Liao, Y. Shao, S. Hao, Y. Huang, Efficient separation and selective Li recycling of spent LiFePO<sub>4</sub> cathode, *Energy Mater.* 3 (2023), <https://doi.org/10.20517/energymater.2023.57>. N/A-N/A.
- [16] T. Yang, D. Luo, A. Yu, Z. Chen, Enabling future closed-loop recycling of spent lithium-ion batteries: direct cathode regeneration, *Adv. Mater.* 35 (2023) 2203218, <https://doi.org/10.1002/adma.202203218>.
- [17] M. Xu, C. Wu, L. Ye, Y. Zhang, C. Zhang, J. Hu, R. Tan, D. Gu, X. Wang, O. Fontaine, C. Zhan, L. Zhuang, X. Ai, J. Qian, Direct regeneration of spent LiCoO<sub>2</sub> black mass based on Fluorenone-mediated lithium supplementation and energy-saving structural restoration, *Adv. Energy Mater.* 14 (2024) 2401197, <https://doi.org/10.1002/aenm.202401197>.
- [18] M. He, X. Jin, X. Zhang, X. Duan, P. Zhang, L. Teng, Q. Liu, W. Liu, Combined pyrohydrometallurgical technology for recovering valuable metal elements from spent lithium-ion batteries: a review of recent developments, *Green Chem.* 25 (2023) 6561–6580, <https://doi.org/10.1039/D3GC01077E>.
- [19] J. Neumann, M. Petranikova, M. Meeus, J.D. Gamarra, R. Younesi, M. Winter, S. Nowak, Recycling of lithium-ion batteries—Current State of the art, circular economy, and next generation Recycling, *Adv. Energy Mater.* 12 (2022) 2102917, <https://doi.org/10.1002/aenm.202102917>.
- [20] P. Zhu, J. Hu, J. Hu, Y. Yang, W. Sun, Y. Yang, G. Zou, H. Hou, X. Ji, Redox-mediated recycling of spent lithium-ion batteries coupled with low-energy consumption hydrogen production, *ACS Energy Lett.* 9 (2024) 569–577, <https://doi.org/10.1021/acseenergylett.3c02256>.
- [21] L. Yang, Z. Gao, T. Liu, M. Huang, G. Liu, Y. Feng, P. Shao, X. Luo, Direct electrochemical leaching method for high-purity lithium recovery from spent lithium batteries, *Environ. Sci. Technol.* 57 (2023) 4591–4597, <https://doi.org/10.1021/acs.est.3c00287>.
- [22] P. Xu, Q. Dai, H. Gao, H. Liu, M. Zhang, M. Li, Y. Chen, K. An, Y.S. Meng, P. Liu, Y. Li, J.S. Spangenberg, L. Gaines, J. Lu, Z. Chen, Efficient direct recycling of lithium-ion battery cathodes by targeted healing, *Joule* 4 (2020) 2609–2626, <https://doi.org/10.1016/j.joule.2020.10.008>.
- [23] K. Jia, J. Ma, J. Wang, Z. Liang, G. Ji, Z. Piao, R. Gao, Y. Zhu, Z. Zhuang, G. Zhou, H.M. Cheng, Long-life regenerated LiFePO<sub>4</sub> from spent cathode by elevating the d-band center of Fe, *Adv. Mater.* 35 (2023) 2208034, <https://doi.org/10.1002/adma.202208034>.
- [24] J. Wang, J. Ma, Z. Zhuang, Z. Liang, K. Jia, G. Ji, G. Zhou, H.M. Cheng, Toward direct regeneration of spent lithium-ion batteries: a next-generation recycling method, *Chem. Rev.* 124 (2024) 2839–2887, <https://doi.org/10.1021/acs.chemrev.3c00884>.
- [25] J. Yan, J. Qian, Y. Li, L. Li, F. Wu, R. Chen, Toward sustainable lithium iron phosphate in lithium-ion batteries: regeneration strategies and their challenges, *Adv. Funct. Mater.* (2024) 2405055, <https://doi.org/10.1002/adfm.202405055> n. d.
- [26] X. Wu, Y. Liu, J. Wang, Y. Tan, Z. Liang, G. Zhou, Toward circular energy: exploring direct regeneration for lithium-ion battery sustainability, *Adv. Mater.* 36 (2024) 2403818, <https://doi.org/10.1002/adma.202403818>.
- [27] K. Jia, G. Yang, Y. He, Z. Cao, J. Gao, H. Zhao, Z. Piao, J. Wang, A.M. Abdelkader, Z. Liang, R.V. Kumar, G. Zhou, S. Ding, K. Xi, Degradation mechanisms of electrodes promotes direct regeneration of spent Li-ion batteries: a review, *Adv. Mater.* 36 (2024) 2313273, <https://doi.org/10.1002/adma.202313273>.
- [28] J. Wang, H. Ji, J. Li, Z. Liang, W. Chen, Y. Zhu, G. Ji, R. Shi, G. Zhou, H.M. Cheng, Direct recycling of spent cathode material at ambient conditions via spontaneous lithiation, *Nat. Sustain.* 7 (2024) 1283–1293, <https://doi.org/10.1038/s41893-024-01412-9>.
- [29] J. Ma, J. Wang, K. Jia, Z. Liang, G. Ji, H. Ji, Y. Zhu, W. Chen, H.M. Cheng, G. Zhou, Subtractive transformation of cathode materials in spent Li-ion batteries to a low-cobalt 5 V-class cathode material, *Nat. Commun.* 15 (2024) 1046, <https://doi.org/10.1038/s41467-024-45091-8>.
- [30] Z. Xing, M. Srinivasan, Electrochemical approach for lithium recovery from spent lithium-ion batteries: opportunities and challenges, *ACS Sustain. Resour. Manag.* 1 (2024) 1326–1339, <https://doi.org/10.1021/acssusresmtg.4c00003>.
- [31] J. Xu, Y. Jin, K. Liu, N. Lyu, Z. Zhang, B. Sun, Q. Jin, H. Lu, H. Tian, X. Guo, D. Shanmukaraj, H. Wu, M. Li, M. Armand, G. Wang, A green and sustainable strategy toward lithium resources recycling from spent batteries, *Sci. Adv.* 8 (2022) eabq7948, <https://doi.org/10.1126/sciadv.abq7948>.
- [32] D. Peng, X. Wang, S. Wang, B. Zhang, X. Lu, W. Hu, J. Zou, P. Li, Y. Wen, J. Zhang, Efficient regeneration of retired LiFePO<sub>4</sub> cathode by combining spontaneous and electrically driven processes, *Green Chem* 24 (2022) 4544–4556, <https://doi.org/10.1039/D2GC01007K>.
- [33] Z. Liu, C. Zhang, M. Ye, H. Li, Z. Fu, H. Zhang, G. Wang, Y. Zhang, Closed-loop regeneration of a spent LiFePO<sub>4</sub> cathode by integrating oxidative leaching and electrochemical relithiation, *ACS Appl. Energy Mater.* 5 (2022) 14323–14334, <https://doi.org/10.1021/acsaem.2c02883>.
- [34] M. Li, R. Mo, A. Ding, K. Zhang, F. Guo, C. Xiao, Electrochemical technology to drive spent lithium-ion batteries (LIBs) recycling: recent progress, and prospects, *Energy Mater* 4 (2024), <https://doi.org/10.20517/energymater.2024.29>. N/A-N/A.
- [35] S. Arnold, J.G.A. Ruthes, C. Kim, V. Presser, Electrochemical recycling of lithium-ion batteries: advancements and future directions, *EcoMat* 6 (2024) e12494, <https://doi.org/10.1002/eom2.12494>.
- [36] Y. Yang, J. Zhang, H. Zhang, Y. Wang, Y. Chen, C. Wang, Simultaneous anodic delithiation/cathodic lithium-embedded regeneration method for recycling of spent LiFePO<sub>4</sub> battery, *Energy Storage Mater.* 65 (2024) 103081, <https://doi.org/10.1016/j.ensm.2023.103081>.
- [37] S. Zhou, J. Du, X. Xiong, L. Liu, J. Wang, L. Fu, J. Ye, Y. Chen, Y. Wu, Direct recovery of scrapped LiFePO<sub>4</sub> by a green and low-cost electrochemical re-lithiation method, *Green Chem.* 24 (2022) 6278–6286, <https://doi.org/10.1039/D2GC01640K>.
- [38] F. Larouche, K. Amouzegar, A. Vjih, G.P. Demopoulos, Ambient-temperature aqueous electrochemical route for direct re-functionalization of spent LFP cathodes of lithium-ion batteries, *J. Power Sourc.* 624 (2024) 235533, <https://doi.org/10.1016/j.jpowsour.2024.235533>.
- [39] S. Chen, B. Zhang, L. Yang, X. Hu, N. Hong, H. Wang, J. Huang, W. Deng, G. Zou, H. Hou, X. Ji, Electrochemical relithiation in spent LiFePO<sub>4</sub> slurry for regeneration of lithium-ion battery cathode, *Inorg. Chem.* 63 (2024) 17166–17175, <https://doi.org/10.1021/acs.inorgchem.4c02844>.
- [40] L. Zhang, Z. Xu, Z. He, Electrochemical relithiation for direct regeneration of LiCoO<sub>2</sub> materials from spent lithium-ion battery electrodes, *ACS Sustain. Chem. Eng.* 8 (2020) 11596–11605, <https://doi.org/10.1021/acssuschemeng.0c02854>.
- [41] T. Yang, Y. Lu, L. Li, D. Ge, H. Yang, W. Leng, H. Zhou, X. Han, N. Schmidt, M. Ellis, Z. Li, An effective relithiation process for recycling lithium-ion battery cathode materials, *Adv. Sustain. Syst.* 4 (2020) 1900088, <https://doi.org/10.1002/advsu.201900088>.
- [42] L. Wang, J. Qiu, X. Wang, L. Chen, G. Cao, J. Wang, H. Zhang, X. He, Insights for understanding multiscale degradation of LiFePO<sub>4</sub> cathodes, *eScience* 2 (2022) 125–137, <https://doi.org/10.1016/j.esci.2022.03.006>.
- [43] Z. Wang, H. Xu, Z. Liu, M. Jin, L. Deng, S. Li, Y. Huang, A recrystallization approach to repairing spent LiFePO<sub>4</sub> black mass, *J. Mater. Chem. A* 11 (2023) 9057–9065, <https://doi.org/10.1039/D3TA00655G>.